

Seeing the order in a mess: optical signature of periodicity in a cloud of plasmonic nanowires

Denys M. Natarov,^{1,*} Marian Marciniak,^{2,3} Ronan Sauleau,⁴
and Alexander I. Nosich¹

¹Laboratory of Micro and Nano-Optics, Institute of Radio-Physics and Electronics NASU, Kharkiv 61085, Ukraine

²National Institute of Telecommunications, 04-894 Warsaw, Poland

³Kielce University of Technology, Faculty of Electrical Engineering, Automatics and Computer Science, 25-314 Kielce, Poland

⁴Institute of Electronics and Telecommunications, IETR UMR CNRS 6164, Université de Rennes 1, 35042 Rennes, France

*den.natarov@gmail.com

Abstract: We consider the two-dimensional (2-D) problem of the H-polarized plane wave scattering by a linear chain of silver nanowires in a cloud of similar pseudo-randomly located wires, in the visible range. Numerical solution uses the field expansions in local coordinates and addition theorems for cylindrical functions and has a guaranteed convergence. The total scattering cross-sections and near- and far-zone field patterns are presented. The observed resonance effects are studied and compared with their counterparts in the scattering by the same linear chain of wires in free space.

©2014 Optical Society of America

OCIS codes: (290.0290) Scattering; (240.6680) Surface plasmons; (280.4788) Optical sensing and sensors.

References and links

1. K. Ohtaka and H. Numata, "Multiple scattering effects in photon diffraction for an array of cylindrical dielectrics," *Phys. Lett.* **73**(5–6), 411–413 (1979).
2. K. T. Carron, W. Fluhr, M. Meier, A. Wokaun, and H. W. Lehmann, "Resonances of two-dimensional particle gratings in surface-enhanced Raman scattering," *J. Opt. Soc. Am. B* **3**(3), 430–440 (1986).
3. S. Zou, N. Janel, and G. C. Schatz, "Silver nanoparticle array structures that produce remarkably narrow plasmon lineshapes," *J. Chem. Phys.* **120**(23), 10871–10875 (2004).
4. R. Gómez-Medina, M. Laroche, and J. J. Sáenz, "Extraordinary optical reflection from sub-wavelength cylinder arrays," *Opt. Express* **14**(9), 3730–3737 (2006).
5. D. M. Natarov, V. O. Byelobrov, R. Sauleau, T. M. Benson, and A. I. Nosich, "Periodicity-induced effects in the scattering and absorption of light by infinite and finite gratings of circular silver nanowires," *Opt. Express* **19**(22), 22176–22190 (2011).
6. D. M. Natarov, R. Sauleau, and A. I. Nosich, "Periodicity-enhanced plasmon resonances in the scattering of light by sparse finite gratings of circular silver nanowires," *IEEE Photon. Technol. Lett.* **24**(1), 43–45 (2012).
7. V. O. Byelobrov, T. M. Benson, and A. I. Nosich, "Binary grating of sub-wavelength silver and quantum wires as a photonic-plasmonic lasing platform with nanoscale elements," *IEEE J. Sel. Top. Quantum Electron.* **18**(6), 1839–1846 (2012).
8. P. Ghenuche, G. Vincent, M. Laroche, N. Bardou, R. Haïdar, J.-L. Pelouard, and S. Collin, "Optical extinction in a single layer of nanorods," *Phys. Rev. Lett.* **109**(14), 143903 (2012).
9. T. V. Teperik and A. Degiron, "Design strategies to tailor the narrow plasmon-photonic resonances in arrays of metallic nanoparticles," *Phys. Rev. B* **86**(24), 245425 (2012).
10. S. R. K. Rodriguez, M. C. Schaafsma, A. Berrier, and J. Gomez Rivas, "Collective resonances in plasmonic crystals: size matters," *Phys. B* **407**(20), 4081–4085 (2012).
11. O. V. Shapoval and A. I. Nosich, "Finite gratings of many thin silver nanostrips: optical resonances and role of periodicity," *AIP Adv.* **3**(4), 042120 (2013).
12. T. L. Zinenko, M. Marciniak, and A. I. Nosich, "Accurate analysis of light scattering and absorption by an infinite flat grating of thin silver nanostrips in free space using the method of analytical regularization," *IEEE J. Sel. Top. Quantum Electron.* **19**(3), 9000108 (2013).
13. D. M. Natarov, R. Sauleau, M. Marciniak, and A. I. Nosich, "Effect of periodicity in the resonant scattering of light by finite sparse configurations of many silver nanowires," *Plasmonics* **9**(2), 389–407 (2014).
14. H. Marinchio, R. Carminati, A. Garcia-Martín, and J. J. Sáenz, "Magneto-optical Kerr effect in resonant subwavelength nanowire gratings," *New J. Phys.* **16**(1), 015007 (2014).

15. B. Auguie and W. L. Barnes, "Diffractive coupling in gold nanoparticle arrays and the effect of disorder," *Opt. Lett.* **34**(4), 401–403 (2009).
16. W. Khunsin and R. Vogelgesang, "Recent advances in nearfield optical analysis and description of amorphous metamaterials," in *Amorphous Nanophotonics*, C. Rockstuhl and T. Scharf, eds., Springer Series Nano-Optics and Nanophotonics (Springer, 2013), pp. 169–200.
17. R. W. Christy and P. B. Johnson, "Optical constants of the noble metals," *Phys. Rev. B* **6**(12), 4370–4378 (1972).

1. Introduction

The periodically structured scatterers, for instance finite chains or arrays of identical dielectric and metal particles, wires and strips attract great attention of researchers in today's nanophotonics. The reason for this is the existence of specific resonant phenomena, among which the most important role is played by the periodicity-caused grating-mode (GM) resonances also called lattice, surface-lattice, and geometrical resonances [1–14]. If the size of the grating element is a fraction of the period, then the GM wavelengths are found just above the Rayleigh wavelengths of the associated infinite gratings [5,12]. The GM-resonances can lead to either almost total reflection or almost total transmission, in a narrow frequency band, of the incident H-polarized plane wave by a sub-wavelength metal wire or strip grating, depending on the spectral distance to the much broader localized surface plasmon (LSP) resonance [5,6,11,12].

In view of the existence of GM resonances, it appears important to clarify how at least a partial periodic structuring makes effect on the scattering by a random ensemble of identical scatterers. This can be interesting both in the nanoantenna and nanosensor applications [15] and in amorphous nanophotonics research [16]. In the course of such study we have noticed that the periodicity of location of sufficiently large number of nanosscatterers has specific "signature" in the TSCS dependences on the wavelength and the incidence angle, visible even if a larger number of similar pseudo-random nanosscatterers is present. This explains the title of our paper: its goal is a demonstration and explanation of the mentioned effect by the example of two-dimensional (2-D) scattering by a cloud of identical metal nanowires of circular cross-section containing the periodicity.

2. Model

We consider the 2-D scattering of the H-polarized plane wave by a finite linear periodic array of M_p silver nanowires hidden inside a cloud of M_c similar nanowires (Fig. 1). The wires are assumed circular with the same radius a . The angle of the plane wave incidence is φ_0 , counted from the plane of array as shown in Fig. 1.

Numerical results presented below relate to the chains of $M_p = 50$ to 200 wires of the 60-nm radius with the period of 450 nm. Around the chain, within the circle of 200 periods in diameter, other $M_c = 200$ wires of the same radius are placed in pseudo-random way. In each case, the random part of the cloud is assumed to be the same. Exact locations of the wire centers of the random part are given in Appendix. The cloud considered is assumed to be sparse: the minimum distance between the random wires is $10.67a$ and the distance between the array part wires is $7.5a$.

To solve a 2-D scattering problem, one has to find the scattered field $H_z(r, \varphi)$. It must satisfy the Helmholtz equation with wavenumber νk_0 where ν is the silver refractive index and k_0 is the free-space wavenumber, or k_0 outside the wires, the tangential field components continuity conditions on wire contours, the radiation condition at infinity, and the condition of the local power finiteness.

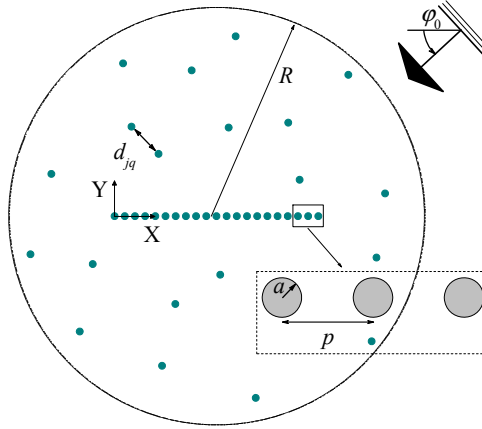


Fig. 1. Sketch of the scattering problem configuration: linear chain of silver nanowires in the cloud of randomly located similar wires.

On expanding the field in the azimuth exponents in the local coordinates, using addition theorems for cylindrical functions, and applying the boundary conditions on all $M = M_p + M_c$ cylinders, we arrive at an $M \times M$ block-type matrix equation where each block is infinite. To ensure that solutions of finite equations with each block truncated to finite order N converge to exact solution if $N \rightarrow \infty$, we cast it to a Fredholm second-kind form [5]. In view of the sparse arrangement of the studied ensemble of nanowires, the block truncation number N can be kept small. In our computations, it has been adapted (from 2 to 4) to provide the 4-digit accuracy in the field expansion coefficients. Mathematical details of the algorithm used can be found in [13]. For the refractive index of silver, we use experimental data of [17].

3. Results

In Fig. 2, presented are reliefs of the normalized by M total scattering cross-section (TSCS) as a function of the angle of incidence and the wavelength, for a cloud of $M_c = 200$ random wires and the same cloud hiding three arrays of $M_p = 50, 100$ and 200 wires.

As known, in the optical range the real part of the silver permittivity ϵ_{Ag} has negative values. This leads to the existence of the LSP natural modes of different azimuthal orders on an infinite sub-wavelength wire. For a single circular silver nanowire in free space all LSP modes cluster, red-shifted, near $\lambda = 338$ nm where $\epsilon_{Ag}(\lambda) = -1$. Because of the losses in silver, the TSCS displays a single broad peak just to the red of this value.

In Fig. 2(a), one can see the bright strip of the LSP resonance along the wavelength of 350 nm for all angles of incidence; no other effects are visible: that means that the wires are not interacting. This is because the whole ensemble is sparse: the minimum inter-wire distance, both in the cloud and in the array, is equal to 7.5 wire radii (see Appendix).

Figure 2(b) shows that the presence of a 50-wire chain inside the cloud changes the relief of the per-wire TSCS considerably so that one can see the appearance of characteristic W-shape “ridge-like” signature for the angle of incidence varying in any of two halfplanes of 0 to 180° and 180° to 360°. This W-shape “ridge” is itself almost mirror-symmetric with respect to 90° and 270° although the contribution of the random wires scattering is slightly different in each quadrant of the plane. It keeps its position and becomes more pronounced if the number of wires in the chain gets larger (see Figs. 2(c) and 2(d)) so that if $M_p = M_c = 200$, the LSP-resonance strip fades off completely relatively to the GM resonance.

For clarity, in Fig. 3(a) presented are the spectra of the normalized TSCS for the angles of incidence $\varphi_0 = 30^\circ, 60^\circ$ and 90° . Comparative results are demonstrated for both the $M_p = M_c = 200$ configuration and for a “bare” linear chain of 200 nanowires in free space.

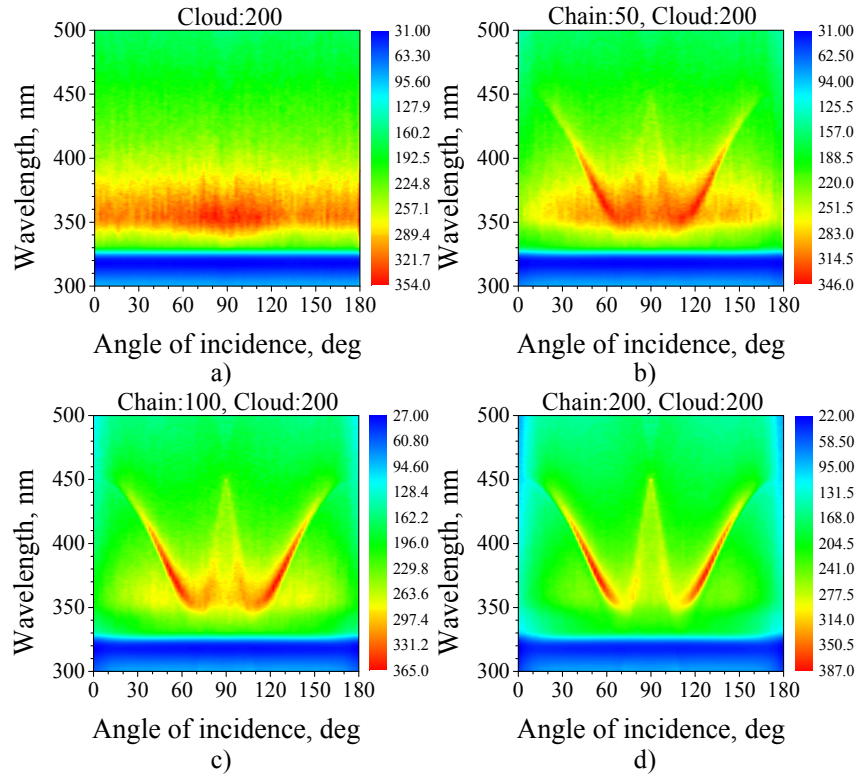


Fig. 2. Reliefs of normalized TSCS (in nm) as a function of the wavelength and the angle of plane-wave incidence for a cloud of 200 randomly located silver nanowires (a) and the same cloud added with different-length periodic arrays of wires (b), (c), (d).

For comparison, we show additionally the spectrum of TSCS of a single silver wire in free space – see the green curve.

In both cases, one can see the effect of the resonances of both types. LSP-resonances are visible near to 350 nm on all curves, i.e. with and without a random cloud. This is not a surprise as LSP-modes are excited on each wire. The effect of the cloud is seen only in the shadowing of the part of wires by those wires, which are better illuminated. This damps the LSP peak in approximately two times. Unlike them, the location of the peaks corresponding to the GM-resonances depends on the angle of incidence (for the fixed period). Of course, GM-resonances for a chain without random cloud have higher peak values; however they are seen at the same wavelengths. Still it is amazing that the addition of random cloud of 200 nanowires does not prevent the GM-resonances to play the leading role and display more intensive peaks than those of the LSP-resonances.

In Fig. 3(b), presented is the relief of the normalized (i.e. per-wire) TSCS as a function of the wavelength and the angle of incidence for the full chain-in-cloud configuration. Note that this is a huge composite scatterer whose total diameter is around 200 wavelengths. The areas of the most intensive scattering stretch along (but do not coincide with) the black dashed lines given by $\lambda_{\pm m}^{RA} = (p/|m|)(1 \pm \cos \varphi_0)$, where $m = \pm 1$ and ± 2 . They are equations of the Rayleigh anomalies for a same-period infinite grating.

This is the expected effect of the presence of periodicity of 200-wire chain, and, what is remarkable it is not spoiled even by the presence of the other 200 wires located randomly. As one can see, the influence of the randomly located wires for the angle of incidence varying in each quadrant of (0-90°), (90°-180°), etc. is very similar to each other. This explains why we

have presented, in Fig. 2, the reliefs of TSCS only for the angle φ_0 varying in the upper half-space.

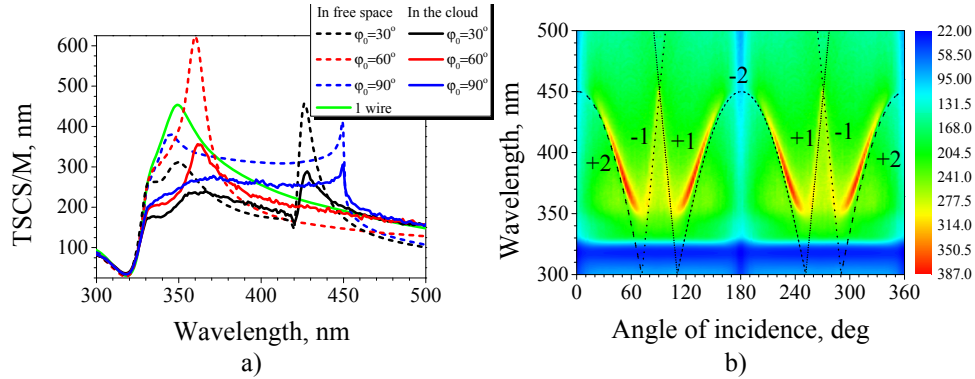


Fig. 3. The wavelength scans of TSCS for different incidence angles φ_0 as compared to the same chain in free space (a) and the relief of TSCS (in nm) normalized by M as a function of the wavelength and the incidence angle of the plane H-wave for the 200 + 200-wire chain-in-cloud configuration (b).

To see the role of the cloud, in Fig. 4 we present both the near-field maps around the center of the chain and the far-field patterns for the 200-wire chain-in-free-space and the chain-in-200-wire-cloud configurations illuminated under the angle of 90° (normal incidence).

For the bare chain one can see a regular standing-wave pattern in the near zone with bright spots corresponding to the ± 1 -st GM fields both at the wires and between them [5,12]. In the cloud, this pattern is still visible, but becomes more complicated because of the influence of non-periodically placed wires around the chain.

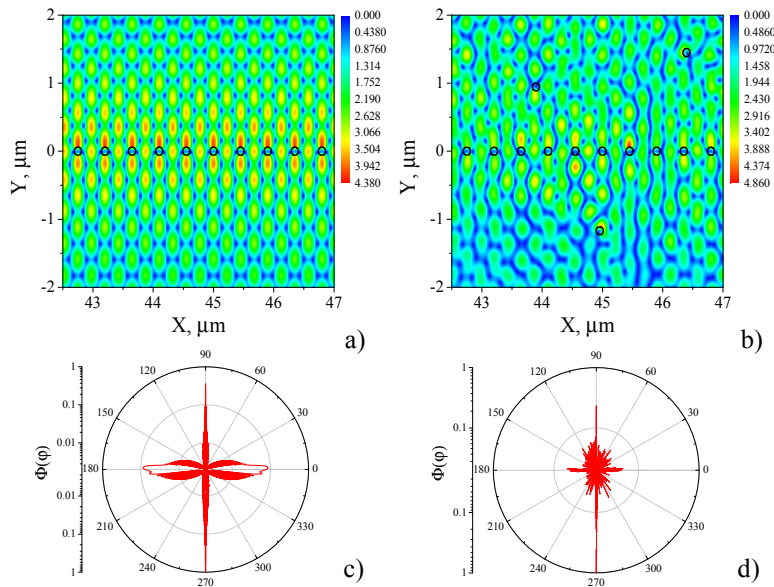


Fig. 4. Near-field maps for 9 central periods and far-field scattering patterns of a linear chain of 200 wires with period 450 nm in free space (a), (c) and 200 + 200-wire chain-in-cloud configuration (b), (d) at the GM-resonance wavelengths of 450.1 nm for the incidence angle of 90° .

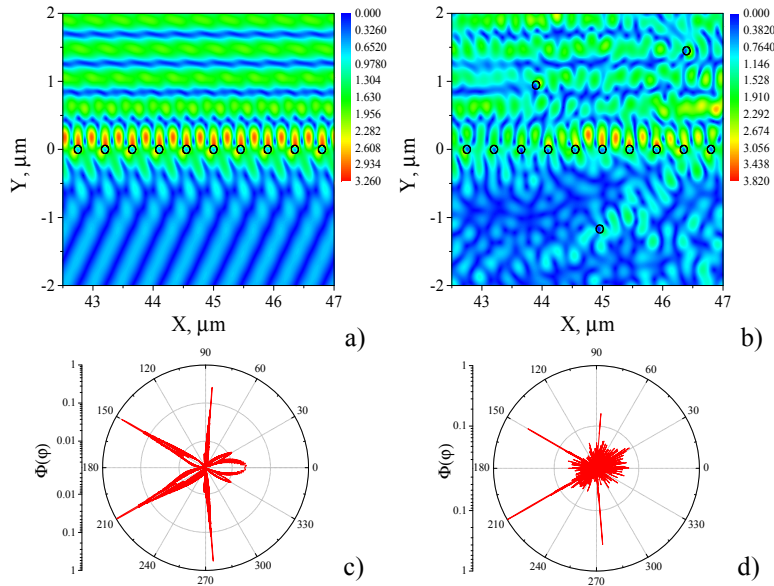


Fig. 5. The same as in Fig. 4 at the GM-resonance wavelengths of 426.4 nm for the incidence angle of 30° .

In the far-field scattering patterns, one can observe the intensive shadow lobe, the specular-reflection lobe (they correspond to the 0-th Floquet harmonics of the corresponding infinite grating) and additionally two wider sidelobes in the directions parallel to the chain. The latter lobes correspond to the grazing propagation of the ± 1 -st Floquet diffractive orders. All these features are still visible if a 200-wire chain is hidden in a 200-wire random cloud although the latter causes a lower-intensity clutter in all directions.

In Fig. 5, the near fields and the far-field scattering patterns are shown for the same two 200-wire chain configurations as in Fig. 4 however at the inclined incidence under $\varphi_0 = 30^\circ$. In this case the + 2-nd GM-resonance wavelength appears just above the Rayleigh wavelength corresponding to the + 2-nd Floquet harmonic (see Figs. 3(a) and 3(b)). Besides of that, the + 1-st harmonic is above the grazing with the angle of propagation close to $\pm 80^\circ$. As a result, a bare chain demonstrates a GM resonance pattern near its center and a standing wave above the chain. In the far field, one can see the intensive and narrow shadow and specular-reflection lobes plus two narrow lobes of the + 1-st Floquet harmonic plus a broader lobe looking at 0° , which corresponds to the + 2-nd harmonic at the grazing.

While the analysis of TSCS tells about the fundamental physics of scattering, the backward scattering cross-section (BSCS), also known as monostatic radar cross-section, is important in the sensing applications. In Fig. 6, we present the wavelength scans of BSCS normalized by Ma at several incidence angles φ_0 for the array of $M_p = 200$ silver wires with period of 450 nm placed in a random cloud of $M_c = 200$ similar wires (Fig. 6(a)) and the relief of the normalized BSCS as a function of φ_0 and λ (Fig. 6(b)). The LSP resonance is well seen as a dip at 350 nm on the curves of BSCS because the light is scattered in the other directions; however it is less visible on the relief where the clutter caused by the random part of the wire collection (i.e. the cloud) is dominant. Still the presence of periodicity is observable. At the normal incidence ($\varphi_0 = 90^\circ$) one can see a dip near 450 nm because considerable part of light escapes in the grazing directions (see Figs. 4 and 5). At the inclined and grazing incidence the Bragg resonances produce strong backscattering 10-20 times above the clutter. Their resonance wavelengths can be derived from the Bragg law, which is, in our

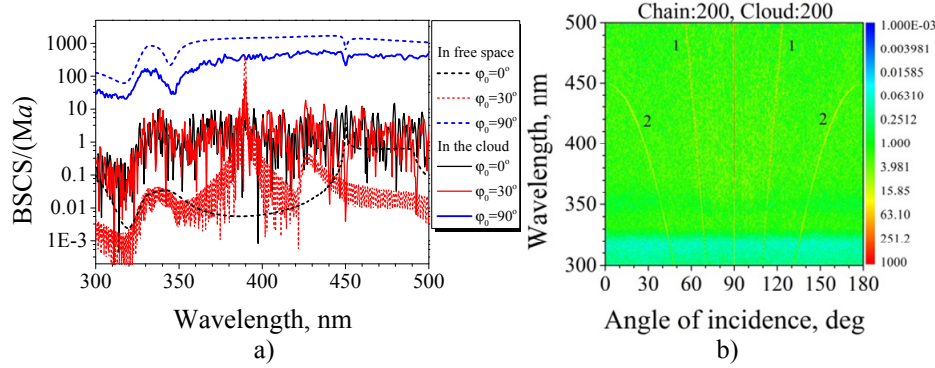


Fig. 6. The wavelength scans of BSCS normalized by Ma for different incidence angles φ_0 (a), and the relief of BSCS as a function of the wavelength and the incidence angle (b). The H-polarized plane wave illuminates a 200 + 200-wire chain-in-cloud configuration with period of 450 nm.

notations, $\lambda_B = 2(p/|s|)\cos\varphi_0$, where $s = 0, \pm 1, \pm 2, \dots$ are the Bragg orders. The bright ridges of high BSCS values marked on the relief in Fig. 6 correspond to the values of $s = 0$ for $\varphi_0 = 90^\circ$ and $\pm 1, \pm 2$ depending on whether φ_0 is smaller or larger than 90° .

5. Summary

Summarizing, in this paper we have presented accurate results for the H-polarized wave diffraction by a sparse chain-in-cloud silver wire configuration. It has been shown that even the presence of a 50-wire periodic chain hidden inside a cloud-like ensemble of 200 pseudo-randomly placed wire scatterers is able to produce well-visible grating-mode resonances in the average per-wire TSCS under any angle of incidence except the grazing angle.

The effect of the periodicity-induced GM-resonance that we have reported shows only little fluctuations if the pseudo-random part of the sparse scattering configuration changes. This is supported by a simple but quite convincing consideration that the V-shape “ridge” on the relief of the TSCS as a function of the incidence angle and the wavelength has the same shape and brightness within each of four complementary quadrants of φ_0 , from 0 to 90° , 180° to 90° , 180° to 270° , and 360° to 270° (see Fig. 3(b)) although the contribution of the random part of configuration is every time different. Similarly one can see the same W-shape “ridge” if making observations within the halfplanes of 0 to 180° and 180° to 360° , on the slightly different random-scattering background. Here, we remind that for the similar array in the free space, the two-fold symmetry results in the fully identical plots or reliefs of TSCS within each of the mentioned four quadrants of φ_0 . As we have demonstrated, if this array is placed into a sparse cloud of random scatterers the found signature of array (in terms of TSCS behavior) is still visible above the appearing “noise.” This is what we call “seeing the order in a mess.”

In the BSCS analysis, the role of the optical signature of periodicity is played by the Bragg-effect maxima while the presence of LSP and GM resonances is hindered.

6. Appendix

As we have explained, each of 200 nanowires of our “cloud” has prescribed however disordered position in a Cartesian system, within the circle of the diameter of $90\ \mu\text{m}$. Into this pseudo-random cloud, we add finite number (50, 100 or 200) of similar wires arranged as a linear chain with the period of 450 nm. The origin of the Cartesian coordinates (x, y) is chosen in the center of the array as shown in Fig. 1. The locations of the wires which make the random-cloud part of the ensemble are the same for each linear array. The coordinates of the

wires which make the array part are the same for the inner 50 wires and are extended periodically along the x -axis to the left and to the right for the 100 and 200-wire arrays.

To make our results reproducible, we give, in Table 1, the coordinates of the center of each wire of the cloud part of the ensemble. Besides, to demonstrate that the cloud is sparse, we give the corresponding values of the minimum separation from the other wires, for each of them. The mean value of the minimum separation happens to be $d_{j(\min)} = 51.64a$, while its maximum value is $128.61a$ and its minimum value is $10.67a$. The mean root square value of $d_{j(\min)}$ is $57.03a$. Note that the separation between the wire centers of the array part of the ensemble is the same for each of three arrays considered and equals $7.5a$.

Table 1. Coordinates of the cloud wire centers and the corresponding minimum separations from other wires (in μm)

No	(x, y)	d_{\min}/a	No	(x, y)	d_{\min}/a	No	(x, y)	d_{\min}/a
1	(-44.64, 0.81)	22.14	68	(10.26, 36.09)	57.69	135	(-23.985, -4.095)	51
2	(-43.695, 3.105)	16.6	69	(11.1825, 25.425)	50.03	136	(-23.49, -22.5)	36.06
3	(-43.38, 4.05)	16.6	70	(11.565, 1.89)	89.72	137	(-22.635, -7.47)	56.54
4	(-42.255, 7.74)	43.69	71	(13.005, 27.81)	50.03	138	(-21.42, -23.13)	36.06
5	(-41.58, 1.53)	36.01	72	(13.455, 17.46)	26.87	139	(-20.61, -14.535)	60.34
6	(-40.59, 5.715)	43.69	73	(13.8375, 19.026)	26.87	140	(-19.485, -8.73)	56.54
7	(-40.05, 3.15)	37.14	74	(14.58, 30.96)	58.7	141	(-18.63, -23.67)	47.36
8	(-38.295, 11.25)	29.7	75	(15.3, 8.64)	76.21	142	(-17.64, -12.465)	60.34
9	(-37.9575, 4.59)	42.34	76	(16.11, 13.14)	18.81	143	(-16.56, -29.925)	74.13
10	(-37.035, 9.99)	29.17	77	(17.145, 13.59)	18.81	144	(-15.3, -15.93)	42.44
11	(-35.82, 8.73)	29.17	78	(17.595, 23.715)	56.03	145	(-14.4225, -4.95)	84.89
12	(-35.1, 3.15)	28.98	79	(18.54, 27.765)	69.31	146	(-13.545, -17.775)	42.44
13	(-34.785, 4.86)	28.98	80	(19.17, 20.745)	56.03	147	(-12.555, -27.99)	36.93
14	(-33.39, 18.99)	92.55	81	(20.295, 5.13)	44.29	148	(-11.25, -9.495)	92.38
15	(-31.567, 0.675)	70.33	82	(21.06, 10.08)	76.05	149	(-10.62, -26.91)	36.93
16	(-31.185, 8.19)	36.28	83	(22.005, 3.096)	44.29	150	(-9.81, -2.79)	84.89
17	(-29.88, 13.41)	63.3	84	(22.86, 24.075)	51.01	151	(-8.73, -37.035)	77.77
18	(-29.295, 7.11)	36.28	85	(24.21, 16.596)	71.97	152	(-7.785, -17.055)	96.75
19	(-28.012, 20.376)	85.47	86	(25.155, 22.05)	51.01	153	(-6.5925, -25.83)	69.5
20	(-26.82, 11.16)	63.3	87	(25.605, 9.675)	76.05	154	(-5.85, -32.49)	72.88
21	(-26.55, 25.74)	83.41	88	(27.18, 25.29)	63.68	155	(-5.31, -10.44)	100.25
22	(-25.74, 5.94)	31.83	89	(27.7425, 19.08)	63.33	156	(-4.095, -36.495)	72.88
23	(-25.155, 14.715)	44.63	90	(28.89, 5.76)	77.84	157	(-2.79, -20.925)	103.44
24	(-24.66, 4.365)	22.37	91	(29.835, 14.94)	58.75	158	(-1.8, -40.455)	32.56
25	(-24.03, 17.145)	44.61	92	(30.69, 11.52)	58.75	159	(-1.26, -14.895)	100.35
26	(-23.355, 4.68)	22.37	93	(30.87, 1.53)	32.93	160	(-0.585, -41.985)	32.56
27	(-22.59, 22.68)	73.7	94	(31.455, 18.27)	61.72	161	(0.18, -1.17)	39.41
28	(-21.645, 18.36)	43.54	95	(32.7825, 1.035)	32.93	162	(0.72, -40.5)	32.95
29	(-19.89, 16.425)	43.54	96	(34.245, 6.21)	45.68	163	(1.62, -5.04)	68.82
30	(-18.99, 32.796)	88.26	97	(34.56, 15.84)	65.71	164	(3.285, -25.38)	82.76
31	(-18.495, 7.875)	96.94	98	(35.8875, 10.26)	53.22	165	(4.05, -20.25)	17.58
32	(-17.235, 20.34)	64.93	99	(36.801, 7.2)	45.68	166	(5.0895, -20.07)	17.58
33	(-15.9075, 13.68)	68.12	100	(37.6875, 3.915)	21.9	167	(5.22, -38.43)	82.55
34	(-13.86, 34.11)	52.8	101	(38.7225, 4.725)	21.9	168	(6.705, -28.98)	78.92
35	(-13.365, 20.79)	64.93	102	(39.42, 10.134)	53.99	169	(7.83, -16.695)	72.46
36	(-12.51, 5.67)	86.47	103	(40.4775, 1.8)	31.7	170	(9.0, -33.48)	80.66
37	(-12.195, 11.97)	59.56	104	(40.7925, 7.2)	53.78	171	(9.81, -20.97)	62.95
38	(-11.3175, 36.0)	52.8	105	(42.0075, 3.78)	28.58	172	(11.43, -29.295)	78.92
39	(-10.305, 18.36)	51.14	106	(42.345, 1.44)	26.75	173	(12.69, -9.495)	99.69
40	(-10.08, 15.3)	51.14	107	(43.3395, 2.7)	26.75	174	(13.455, -19.98)	62.95
41	(-9.54, 22.59)	29.86	108	(44.46, 0.495)	19.81	175	(14.715, -2.475)	89.72
42	(-8.6625, 12.51)	52.16	109	(-44.595, -0.517)	16.77	176	(16.29, -15.48)	66.09
43	(-8.199, 40.05)	71.44	110	(-43.695, -0.967)	10.67	177	(17.01, -24.975)	63.3
44	(-7.7625, 22.815)	29.86	111	(-43.065, -1.08)	10.67	178	(18.135, -11.97)	66.09

45	(-7.6275, 7.425)	58.87	112	(-42.435, -1.507)	12.69	179	(19.26, -21.915)	63.3
46	(-6.93, 19.584)	55.61	113	(-41.94, -2.385)	16.79	180	(20.7225, -5.9085)	99.44
47	(-5.8725, 36.45)	71.44	114	(-41.139, -0.585)	26.51	181	(22.005, -14.445)	63.06
48	(-5.1075, 9.9)	58.87	115	(-40.32, -3.69)	22.25	182	(23.715, -11.07)	39.86
49	(-4.3425, 14.58)	14.43	116	(-39.6765, -2.52)	22.25	183	(25.155, -0.99)	85.99
50	(-3.555, 14.94)	14.43	117	(-38.205, -3.465)	29.15	184	(25.515, -9.495)	39.86
51	(-2.5605, 6.57)	69.87	118	(-37.485, -9.5985)	58.8	185	(27.72, -20.9475)	128.61
52	(-2.43, 30.555)	113.78	119	(-36.765, -1.62)	39.01	186	(29.565, -13.455)	69.07
53	(-1.7775, 42.39)	103.04	120	(-36.18, -13.14)	62.9	187	(30.915, -7.245)	79.8
54	(-0.8775, 0.945)	39.41	121	(-35.2305, -6.885)	40.6	188	(31.815, -1.53)	45.69
55	(-0.09, 23.76)	67.5	122	(-34.56, -4.455)	42.01	189	(33.705, -13.275)	51.87
56	(1.17, 9.405)	46.33	123	(-33.795, -9.495)	49.65	190	(34.605, -10.296)	51.87
57	(1.62, 1.449)	42.46	124	(-32.805, -6.66)	40.6	191	(35.865, -5.445)	22.06
58	(2.52, 6.975)	46.33	125	(-31.68, -12.645)	20.52	192	(36.945, -6.21)	22.06
59	(2.97, 38.43)	103.04	126	(-31.297, -11.475)	20.52	193	(38.205, -2.34)	17.4
60	(3.96, 23.715)	67.5	127	(-30.285, -7.56)	44.6	194	(39.0375, -1.71)	17.4
61	(5.4, 19.8)	47.63	128	(-29.655, -14.175)	25.5	195	(40.095, -9.9)	63.06
62	(6.255, 15.75)	54.54	129	(-28.71, -2.43)	61.78	196	(40.815, -3.015)	36.75
63	(6.66, 32.715)	27.01	130	(-28.305, -13.455)	25.5	197	(41.805, -6.525)	60.78
64	(7.0425, 31.14)	27.01	131	(-27.36, -20.34)	57.9	198	(43.02, -0.99)	18.81
65	(7.965, 18.54)	47.63	132	(-26.685, -5.535)	51	199	(44.055, -1.44)	18.81
66	(8.73, 7.38)	102.98	133	(-25.965, -15.84)	30.64	200	(45.045, -0.54)	19.81
67	(9.315, 32.76)	44.26	134	(-25.29, -17.55)	30.64			